ELSEVIER

Journal of Organometallic Chemistry 658 (2002) 266–273

Journal of Organometallic Chemistry

www.elsevier.com/locate/jorganchem

# Two nickelocenes and ferrocene in a rigid *cis*/*trans* chain

Martin Herker [a], Frank H. Köhler [a,*], Markus Schwaiger [b], Bernd Weber [a]

[a] *Anorganisch-Chemisches Institut, Technischen Universität München, Lichtenbergstrasse 4, D-85747 Garching, Germany*
[b] *Institut für Organische Chemie und Biochemie der, Technischen Universität München, Lichtenbergstrasse 4, D-85747 Garching, Germany*

Received 4 March 2002; received in revised form 2 May 2002; accepted 2 May 2002

**Abstract**

With the aim of studying the conformation of bridged paramagnetic metallocenes and the conformation-dependent electron spin delocalization therein, a trimetallic model compound was synthesized. First, a nickelocene bonded to cyclopentadienyl (Cp) anion by two $SiMe_2$ groups was made in three steps. Further reaction with solvated iron dichloride gave a trimetallic metallocene (**6**) that had the metal sequence NiFeNi. X-ray crystal analysis revealed that in one-half of **6** the arrangement of the metal atoms Ni and Fe with respect to the ligand bridge was *trans*; in the other half it was *cis*. The Cp ligands were neither staggered nor eclipsed, the metallocene axes were slightly bent, and bending was also observed about three vectors in the bridging ligand. The $^{1}H$-, $^{13}C$-, and $^{29}Si$-NMR spectra were in accord with two unpaired electrons per nickelocene, with both *cis* and *trans* arrangement of the metal atoms, and with bending of the ligand bridges. Large NMR signal shifts indicated transfer of spin density from the nickelocenes into the $SiMe_2$ bridges and the central ferrocene. The efficiency of the spin transfer was found to depend on the bending angle of the ligand bridge. MO calculations illustrated that spin delocalization in the *cis* half of **6** was less pronounced than in the *trans* half.


*Keywords:* Nickelocene; Ferrocene; Bridged cyclopentadienyls; NMR spectroscopy; Electron spin delocalization

## 1. Introduction

Linking metallocenes (most often ferrocenes) by a single bridge per cyclopentadienyl (Cp) ligand can lead to organometallic polymers [1]. These compounds would be conformationally very flexible as has been found for oligomeric ferrocenes by, for instance, *one* $Me_2Si$ group per Cp [2]. When the bridging is effected by *two adjacent* groups per Cp the resulting molecules are more rigid, and various more stable geometric motifs become available. A widely studied example is the dianion **1** [3] which forms two pentahapto bonds to metals thereby yielding the structurally established motifs A [4], B [3,5], C [6], D [5], and E [6c] in Fig. 1. In these motifs the bar is a Cp in side view, and M represents a fragment consisting of a metal ion and auxiliary ligands.

For motif C additional isomers are possible if different fragments (M and M′) and/or more than two fragments are bridged. For instance, trinuclear metallocenes derived from the bridging ligand **1** should be able to adopt conformations F, G, and H (Fig. 2), regardless whether M and M′ are equal or not. The arrangement of M and M′ in conformation H is particularly interesting, because it is the only one that would lead to small rings if no ligand other than the bridging one were present. This has actually been found in a ring, which contains seven ferrocenes (Fig. 3) [7]. On the other hand, only conformer F could be isolated when a vanadocene was flanked by two ferrocenes, i.e. when the metal sequence was FeVFe [6d]. This suggests that the different M–Cp distances of the metallocenes [8] have some bearing on the formation of conformers F, G, and H. Actually, the steric hindrance between the axial methyl groups at the silicon bridges and adjacent Cp protons (see frames in Fig. 4) must be considered: if the M–Cp distances of the central and terminal metallocenes are long and short (Fig. 4, F′), respectively, steric hindrance is small. This scenario has been realized with the metal sequence FeVFe [6d]. Fig. 4, F″ shows the reverse case where

* Corresponding author. Tel.: +49-89-28913109; fax: +49-89-28913762
*E-mail address:* f.h.koehler@lrz.tu-muenchen.de (F.H. Köhler).

0022-328X/02/$ - see front matter 
PII: S0022-328X(02)01674-1

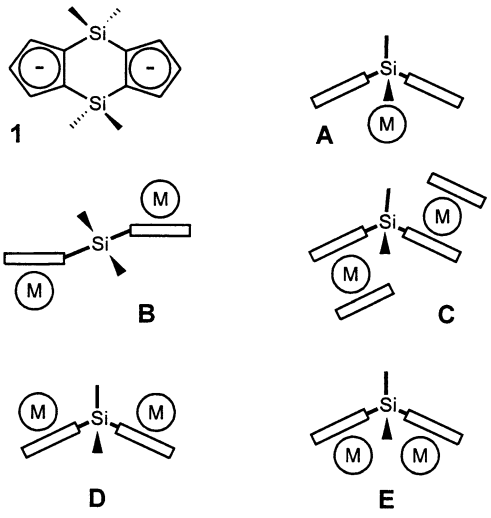


Fig. 1. Metal binding motifs of ligand **1**.

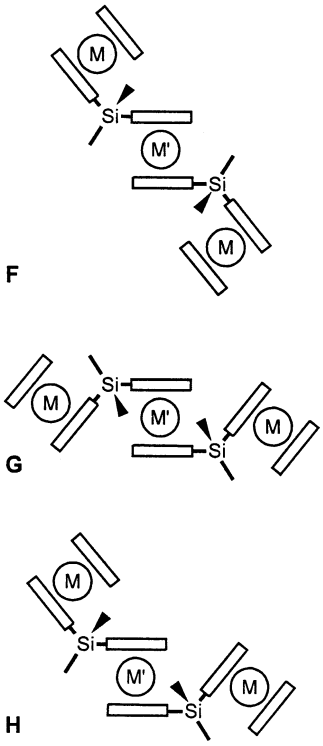


Fig. 2. Conformers of three metallocenes bridged by four silyl groups of two ligands **1**.

the M–Cp distance of the central metallocene is shorter than that of the terminal ones and where steric hindrance is stronger. The latter type of compounds is expected to prefer conformation G with less steric repulsion. While the conformational variety is interesting in itself, it is expected to influence the distribution of the unpaired electrons in such molecules, and this in turn has been shown to influence the magnetic interaction in compounds with adjacent paramagnetic metallocenes [6d]. In the present work, we wanted to check

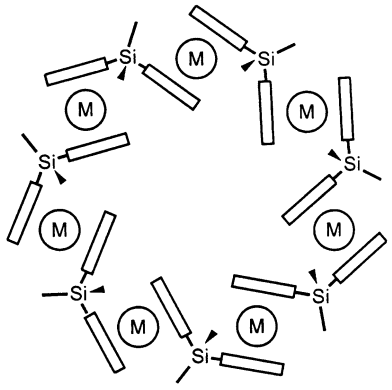

Fig. 3. Sketch of seven bridged ferrocenes forming a ring.

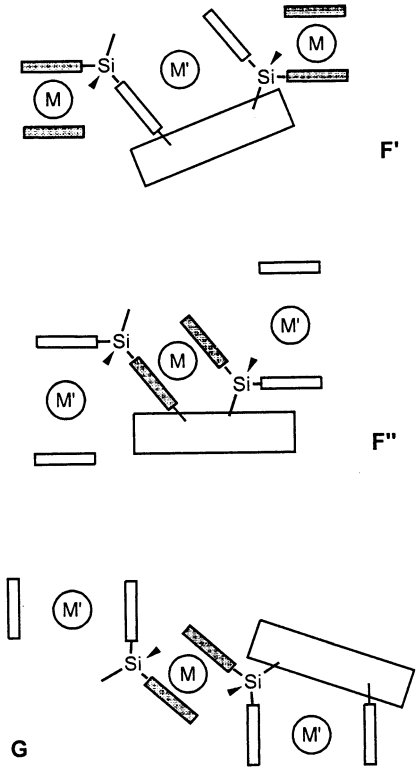


Fig. 4. Steric interactions between the framed parts of trimetallic bridged metallocenes depending on the M–Cp distance and the metallocene sequence. The differences of the M–Cp distances are exaggerated.

whether conformation G can be realized with the metal sequence NiFeNi and how the unpaired electrons would be delocalized.

## 2. Results and discussion

### 2.1. Synthesis

The assembly of different metals in trinuclear bridged metallocenes such as the target molecule **6** (Scheme 1) is based on the stepwise deprotonation of the starting

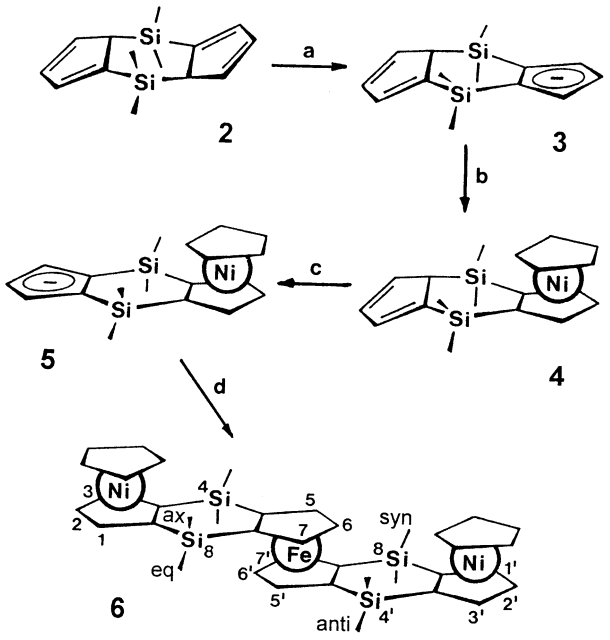


Scheme 1. Synthesis of compound **6**. (a) *n*-BuLi; (b) CpNa, $NiBr_2(THF)_{1.5}$; (c) lithium piperidid; (d) $FeCl_2(THF)_{1.5}$. Only one of two isomers is shown for **2** and **4**.

ligand precursor **2**. Thus, removal of one proton gave anion **3** [3], which was converted to the mixed-ligand nickelocene **4** [9]. Compound **4** was formed together with $Cp_2Ni$ and a nickelocene, which had two ligands **3**. The yield of the latter nickelocene was kept low by using an excess of CpNa in step b; it formed insoluble coordination polymers after steps c and d and was not studied further. The other nickelocenes were separated from ionic impurities by extraction with hexane before mild deprotonation was achieved in step c. Anion **5** and $Cp_2Ni$ were separated by extracting the latter with hexane so that, after step d, the only product soluble in hexane was expected to be **6**. Actually, some $Cp_2Ni$ and **4** had to be removed from **6** by medium pressure chromatography. When the volume of a toluene solution of **6** was slowly reduced, crystals containing one solvent molecule per formula unit were obtained.

### 2.2. Crystal structure of 6

After prolonged standing of a saturated solution of **6** in benzene-$d_6$, solvent-free crystals were obtained wherein **6** has the molecular structure shown in Fig. 5. It turns out that both the *cis* and *trans* arrangement of the nickel and iron atoms relative to the bridging ligand are realized, that is, motifs D and C of Fig. 1, respectively. Since different neighboring metallocenes are present, it is not sufficient to classify the *trans* side of **6** as C; there is still a choice between the *trans* versions of motifs F and G in Fig. 2. As expected, in **6** the metal–Cp centroid distances of the ferrocene moiety (average

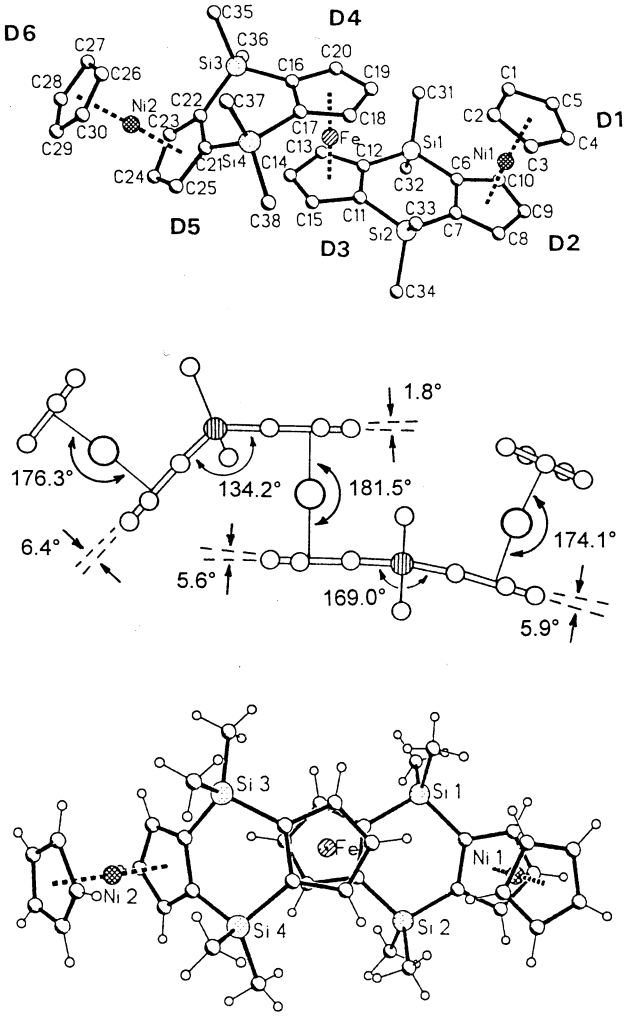


Fig. 5. Molecular structure of compound **6** (top and bottom: ORTEP drawings, middle: sketch showing interplane angles).

1.65 Å) is smaller than that of the nickelocene moieties (average 1.82 Å). The steric constraints outlined in Fig. 4 would, therefore, favor motif G which has actually been found. Compound **6** features various distortions that are also illustrated in Fig. 5. Thus, there are interplane angles of 1.8–6.4° at the junctions between the Cp rings and the adjacent halves of the six-membered rings, and all metallocene moieties are slightly bent (1.5–5.9°). Quite remarkably, the bending about the Si, Si vector is smaller for the *cis* than for the *trans* arrangement (complementary angles: 169.0 and 134.2°, respectively). In consequence, there are axial and equatorial methyl groups on the *trans* side of **6**, while on the *cis* side the methyl groups are neither axial nor equatorial, but *syn* and *anti* with respect to the adjacent nickelocene. It can be seen at the bottom of Fig. 5, that the molecular symmetry is low ($C_1$), that is, the two ferrocene ligands are not staggered. However, with a twist angle of 15.9° they are not eclipsed either. Intermediate twist angles (19.0 and 18.0°) also exist for

Table 1
Selected bond distances (Å) and angles (°) of compound **6** with eds's in units of the last significant figure in parentheses

| | | | |
|---|---|---|---|
| *Bond distances* | | | |
| Si1–C6 | 1.855(6) | Si3–C16 | 1.837(7) |
| Si1–C12 | 1.863(6) | Si3–C22 | 1.866(6) |
| Si1–C31 | 1.861(8) | Si3–C35 | 1.863(7) |
| Si1–C32 | 1.872(7) | Si3–C36 | 1.844(7) |
| Si2–C7 | 1.854(6) | Si4–C17 | 1.867(7) |
| Si2–C11 | 1.844(7) | Si4–C21 | 1.863(7) |
| Si2–C33 | 1.842(8) | Si4–C37 | 1.858(7) |
| Si2–C34 | 1.878(7) | Si4–C38 | 1.858(7) |
| Ni1–D1 [a] | 1.826 | Fe–D3 [a] | 1.657 |
| Ni1–D2 [a] | 1.814 | Fe–D4 [a] | 1.653 |
| Ni2–D5 [a] | 1.815 | Ni2–D6 [a] | 1.822 |
| *Bond angles* | | | |
| C6–Si1–C12 | 107.0(3) | C16–Si3–C22 | 104.1(3) |
| C31–Si1–C32 | 107.2(4) | C35–Si3–C36 | 108.8(4) |
| C7–Si2–C11 | 107.0(3) | C17–Si4–C21 | 104.2(3) |
| C33–Si2–C34 | 106.7(4) | C37–Si4–C38 | 108.6(4) |

[a] D is the centroid of the respective Cp ring (see Fig. 5).

the Cps of the nickelocenes on the *cis* and *trans* side, respectively. Further selected structural data are given in Table 1.

### 2.3. $^{1}H$-, $^{13}C$-, and $^{29}Si$-NMR spectra

In solution $C_s$ symmetry follows from all NMR spectra. As compared to the signal sets known [6d] for motif F in Fig. 2 (*trans*, *trans* conformer), there is a doubling of the signal number owing to *cis* and *trans* moieties. But there are no further signals that would imply $C_1$ symmetry. As can be seen from the data in Table 2, the $^{1}H$- and $^{13}C$-NMR signals appear in ranges that are known from simpler analogues containing two nickelocenes (*cis*- and *trans*-NiNi) or one ferrocene and one nickelocene (FeNi) [10]. For instance, the nickelocene proton signals are shifted more than 200 ppm to low frequency. Although the signals are broad (up to 1400 Hz) the non-equivalent protons are resolved except for those of the terminal Cps which coincide accidentally. The nickelocene carbon atoms, which are expected to show extremely broad signals above 1000 ppm [11] were not considered, because the signal-to-noise ratio was too low. As outlined in Section 3, the NMR signal shifts in Table 2 are contact shifts, $\delta^{con}$.

The detailed signal assignment was of interest, because from the signal shifts it can be concluded how the structure determines the transfer of the unpaired electron spin density from one metallocene to the next. The strongly shifted nickelocene protons were assigned by comparison with *cis*- and *trans*-NiNi [10], and the same applies for the methyl protons except for the

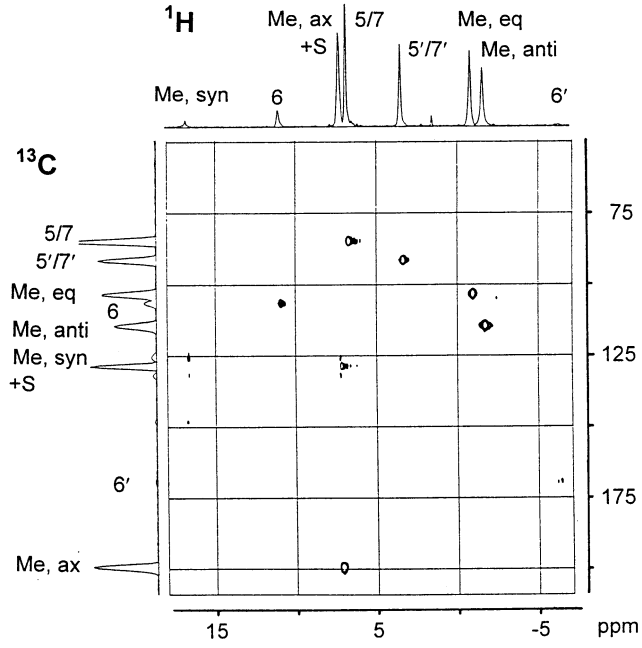


Fig. 6. HMQC NMR spectrum of compound **6** (500.12 MHz, benzene-$d_6$, 298 K). S, solvent.

Table 2
$^{1}H$ and $^{13}C$ contact shifts [a] of compound **6**

| Position of nucleus [b] | $\delta^{con}(^{1}H)$ | $\delta^{con}(^{13C}H)$ | Position of nucleus [b] | $\delta^{con}(^{1}H)$ | $\delta^{con}(^{13}C)$ |
|---|---|---|---|---|---|
| Cp | −259 | [c] | Cp′ | −259 | [c] |
| 2 | −239 | [c] | 2′ | −231 | [c] |
| 1/3 | −244 | [c] | 1′/3′ | −233 | [c] |
| 3a/8a | | [c] | 3a′/8a′ | | [c] |
| 4a/7a | | 144.6 | 4a′/7a′ | | 2.1 |
| 5/7 [d] | −1.1 | 16.6 | 5′/7′ [d] | 2.1 | 9.6 |
| 6 | −11.7 | 98.8 | 6′ | 5.8 | 33.6 |
| $Me_{ax}$ | 6.5 | 200.1 | $Me_{syn}$ | 16.7 | 121.2 |
| $Me_{eq}$ | 1.7 | 104.0 | $Me_{anti}$ | −2.6 | 115.8 |

[a] In ppm at 298 K.
[b] For numbering see Scheme 1.
[c] Not observed.
[d] Interchange of signal assignment for positions 5/7 and 5′/7′ not excluded.

distinction of $Me_{eq}$ and $Me_{anti}$ (see below). A HMQC spectrum established the C, H connectivities of the methyl groups and the ferrocene moiety. While Fig. 6 shows all expected cross peaks, their intensities vary. This is due to the unpaired electrons which entail rather different relaxation times, $T_1$, of the various nuclei [12]; in particular, $T_1$ of the nuclei not shown in Fig. 6 is so short that their C, H correlations are quenched. The one-dimensional $^{13}$C-NMR spectrum shows two additional signals (at 222.0 and 79.5 ppm) which belong to the quarternary carbon atoms C4a/7a and C4a′/7a′. The primed and non-primed nuclei may be distinguished by comparison with the NMR data of the dinuclear species NiFe [10]. While this works well for C4a/7a and C4a′/7a′, it cannot be excluded that the assignment of the protons and carbon atoms in positions 5–7 and 5′–7′ must be interchanged. But this does not touch on the discussion of the spin delocalization below.

The most simple spectroscopic proof for two different bridging ligands in **6** is the $^{29}$Si-NMR spectrum. It shows two signals that are shifted −839 and −879 ppm, a range that is characteristic of adjacent nickelocene and ferrocene moieties [9]. The assignment to Si4/8 and Si4′/8′ is too speculative, even after comparison with *trans*-NiNi and FeNi.

### 2.4. Spin delocalization

It is well known that in nickelocenes positive spin density is delocalized into the Cp π orbitals [13], while a subsequent polarization step induces negative spin density on the Cp protons. Since the contact shifts are proportional to the spin density on the observed nucleus, the negative signal shifts of the Cp protons of **6** confirm the expected delocalization. There is also delocalization of spin density into the $SiMe_2$ bridges and further into the ferrocene moiety, as can be seen from the considerable contact shifts of the corresponding nuclei. It has been discussed in detail previously, that this delocalization depends on the bending about the Si, Si vectors of the bridging ligands as illustrated in Fig. 2 [6d]. The bending is related to the dihedral angle, $\theta$ that a given Si–C bond forms with the spin-containing Cp π orbital of the nearest nickelocene, for instance, the dihedral angle between Si8–$Me_{ax}$, Si8–$Me_{eq}$, and Si8–C7a with the normal passing through C8a. The relation to the contact shift is given by [13]

$$\delta^{con} = \delta_0 + B\cos^2\theta \quad (1)$$

where the angle-dependent term is also known as hyperconjugative contribution, and where $\delta_0$ comprises all other shift contributions. The validity of Eq. (1) for the results of the methyl groups was checked by tentatively using the dihedral angles of the solid-state structure of **6**. As can be seen in Table 3, the contact shifts nicely parallel the term $\cos^2\theta$, which means that the bending of **6** in solution and the solid-state is similar. From the $^{13}$C-NMR data of $Me_{ax}$ and $Me_{eq}$ and Eq. (1), a hyperconjugative shift contribution of $B = 121.6$ ppm and $\delta_0 = 80.4$ ppm are obtained. When $B$ is maintained for $Me_{syn}$ and $Me_{anti}$, a mean value of $\delta_0 = 29.1$ results. The difference of the $\delta_0$ values must be ascribed to slightly different metal–Cp bonding in the nickelocene moieties. The agreement of all values is much better, when the carbon signal of $Me_{anti}$ is more shifted than that of $Me_{eq}$. Then the pending distinction of the proton signals of $Me_{anti}$ and $Me_{eq}$ follows from the C, H correlation.

Table 3
Dihedral angles ($\theta$) and contact shifts of the methyl groups of compound **6**

| | $Me_{ax}$ | $Me_{eq}$ | $Me_{syn}$ | $Me_{anti}$ |
|---|---|---|---|---|
| $\theta$ (°) | 5.9 | 63.8 | 30.8 | 31.3 |
| $\cos^2\theta$ | 0.989 | 0.195 | 0.738 | 0.730 |
| $\delta^{con}$($^{13}$C) (ppm) | 200.1 | 104.0 | 121.2 | 115.8 |
| $B$ (ppm) | 121.0 | 121.0 | 121.0 | 121.0 |
| $\delta_0$ (ppm) | 80.4 | 80.4 | 29.7 | 29.7 |

The geometry also determines the spin transfer from paramagnetic to diamagnetic metallocenes. Thus, it has been shown previously [6d] that the spin transfer should increase with increasing bending of the bridging ligand, although a proof based on both NMR and crystal data was missing. In compound **6**, the bending angles of the *cis* and *trans* side (deviation from coplanarity: 11.0 and 45.8°, respectively) are associated with contact shifts of 2.1 (C4a′/7a′) and 144.6 ppm (C4a/7a), respectively. This establishes that bending of the bridge is a means of tuning the spin delocalization into adjacent metallocenes.

The effect of bending of **6** on the spin density distribution is reflected in the singly occupied molecular orbitals (SOMOs), because the squared atomic orbital coefficients are a measure of the spin densities at the respective atoms. To illustrate this, the four SOMOs of **6** obtained from Extended Hückel calculations are given in Fig. 7. When the contributions of all SOMOs are added, it is obvious that spin density appears at the methyl carbon atoms and at the Cp ligands of the central ferrocene. In addition, it is confirmed that more spin density resides on the Cp belonging to the more strongly bent *trans* side of **6** than on the Cp belonging to the *cis* side.

### 2.5. Conclusions

Two nickelocenes can be bonded to each Cp of ferrocene via $SiMe_2$ groups to yield the bridged metallocene **6** featuring the metal sequence NiFeNi. The solid-state structure confirms the hypothesis that steric interaction between the methyl groups of the $SiMe_2$

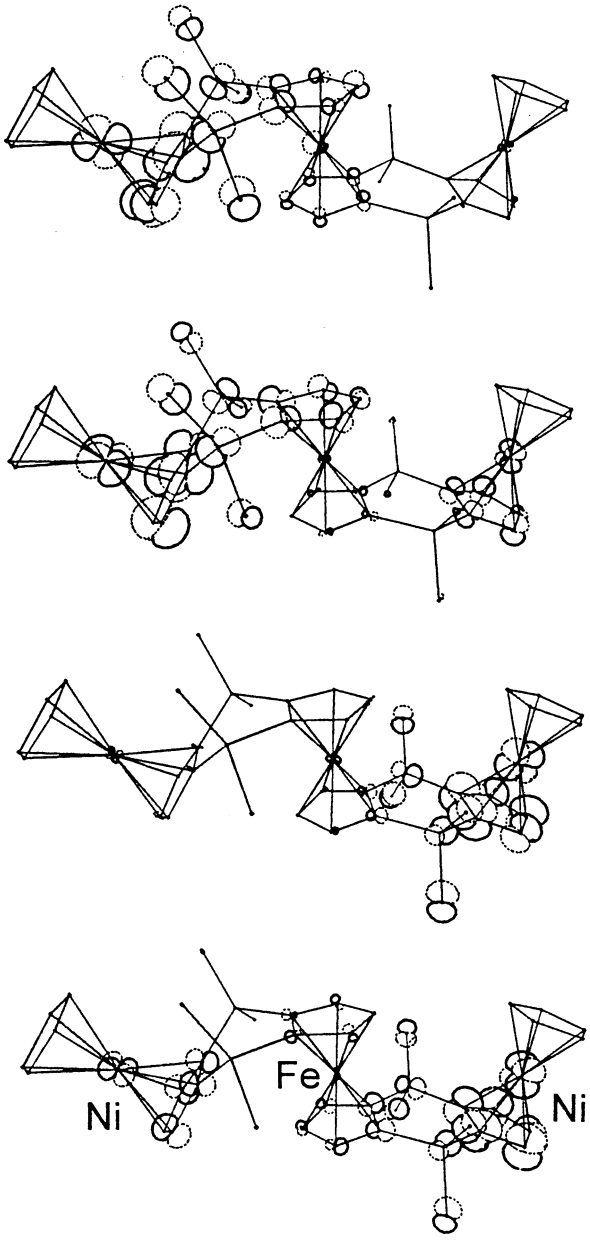


Fig. 7. Three-dimensional contour plots of the molecular orbitals reflecting the spin distribution in compound **6**. All hydrogen atoms and the AO contributions of the terminal Cps have been omitted for clarity.

bridges and the Cp ligands—modulated by the metal–Cp distance—determines the relative orientation of next-neighbor metallocenes. However, this is only realized for one half of **6** where Ni and Fe are *trans* relative to the bridging ligand. In the second half of **6** a *cis* arrangements is adopted. Compound **6** experiences various distortions, most notably different bending of the ligand bridges: it is strong and weak on the *trans* and *cis* side of **6**, respectively.

In solution most distortions are averaged out, but the bending persists. This follows from the $^{1}$H-, $^{13}$C-, and $^{29}$Si-NMR spectra, which also prove that the spin transfer from one metallocene to the next is more efficient when the ligand bridge is bent, rather than flat. Additional spin transfer occurs to the methyl groups of the $SiMe_2$ links. The spin delocalization can be visualized by MO calculations, and the correlation between the molecular geometry and spin delocalization follows a simple law.

## 3. Experimental

All manipulations were carried out under purified dinitrogen by using Schlenk techniques and solvents dried by standard methods and distilled under dinitrogen. Medium pressure liquid chromatography (MPLC) was carried out with an apparatus from Kronwald, the mass and NMR spectra were recorded with Finnigan MAT (electron impact mode, 70 eV) and JEOL JNM GX 270, Bruker MSL 300 as well as AMX 500 spectrometers, respectively. The experimental NMR signal shifts, $\delta^{exp}$, were measured relative to the solvent signals (dioxane-$d_8$: $\delta(^{1}H) = 3.53$, $\delta(^{13}C) = 66.6$) and to internal hexamethyldisiloxane ($\delta(^{29}Si) = 6.9$). The paramagnetic signal shifts, $\delta^{para}$, were obtained by subtracting from $\delta^{exp}$ the corresponding signals of the analogous *cis*, *trans* diiron derivative [14]. As the g-factor anisotropy of nickelocenes is small [15], dipolar shift contributions to $\delta^{para}$ are also small, so that the $\delta^{para}$ values can be considered to be contact shifts, $\delta^{con}$ [16]. All spectra were recorded at 293 K, and the $\delta^{para}$ values were converted to those at the standard temperature of 298 K by using the relationship $\delta^{con} \propto T^{-1}$. The elemental analyses were carried out by the microanalytical laboratory of the authors institution.

### 3.1. *cis,trans*-Bis(cyclopentadienylnickel)-bis(μ-1,2,3,3a,8a-$\eta^5$-tetrahydro-4,4,8,8,-tetramethyl-4,8-disila-*s*-indacene-3a,7a-diyl)iron (**6**)

A solution of *n*-BuLi in $C_6H_{14}$ (5.5 ml, 2.53 M) was added dropwise to 3.41 g (13.95 mmol) of **2** [3] dissolved in 50 ml of THF and cooled to −55 °C. The reaction mixture was stirred for 6 h and allowed to reach room temperature. After addition of CpNa dissolved in THF (28 ml, 0.98 M) and of 10.0 g (32 mmol) of $NiBr_2(THF)_{1.5}$ the reaction mixture turned green. It was stirred overnight, the solvents were removed under reduced pressure, and the solid remainder was extracted with three portions of 80 ml of $C_6H_{14}$. The combined green extracts were cooled to −78 °C, and 12.5 mmol of cold (−78 °C) lithium piperidid (freshly prepared from 1.3 ml of piperidine in 10 ml of $C_6H_{14}$ and 5 ml of a 2.53 M solution of *n*-BuLi in $C_6H_{14}$) were added. After stirring for 1 day at −78 °C and warming to 25 °C during 8 h, a light-green precipitate and a green solution

Table 4
Crystal data and structure refinement for compound **6**

| | |
|---|---|
| Empirical formula | $C_{38}H_{46}FeNi_2Si_4$ |
| Formula weight | 788.38 |
| Crystal color | Green |
| Crystal system | Monoclinic |
| Space group | $P2_1$ |
| Cell dimensions | |
| $a$ (Å) | 9.09(1) |
| $b$ (Å) | 16.0039(1) |
| $c$ (Å) | 14.600(1) |
| $\beta$ (°) | 107.19(1) |
| $V$ (Å$^3$) | 2143.3(3) |
| $Z$ | 2 |
| $D_{calc}$ (g cm$^{-1}$) | 1.222 |
| Crystal size (mm) | 0.45 × 0.25 × 0.20 |
| $\theta$ Range (°) | 3–26 |
| Reflections collected | 8447 |
| Reflections observed | 7404 |
| Independent reflections | 7991 [$R_{int} = 0.0201$] |
| Final $R$ values [$F_0 > 4\sigma(F_0)$] | $R_1 = 0.0578$, $wR_2 = 0.1837$ |
| $R$ values (all data) | $R_1 = 0.0648$, $wR_2 = 0.1912$ |

had formed. The solution was removed via cannula; the precipitate was washed twice with $C_6H_{14}$ and dissolved in 50 ml of THF. To the green solution was added a suspension of 2.31 g (9.80 mmol) of $FeCl_2(THF)_{1.5}$ in 50 ml of THF whereupon the color lightened. After stripping the solvents a light-green powder was obtained which was dissolved in $C_6H_{14}$ and subjected to MPLC. From the silica used as stationary phase (Merck Silica 60, 15–40 mesh) water was removed at 200 °C and $10^{-2}$ bar, and oxygen-free water was added; this procedure was repeated three times. On the column (26 mm diameter, 50 cm length) at 20 bar three green bands developed with $C_6H_{14}$ as eluent. The first and second band contained $Cp_2Ni$ and compound **4**, respectively. After elution of the third band the solvent was stripped, and the solid was recrystallized from $C_6H_5CH_3$ to give 2.36 g of an olive–green powder that analyzed for **6** × $C_6H_5CH_3$ (yield 38.4% relative to **2**).

No m.p. was observed up to 200 °C where decomposition to a brown solid occurred. Found: C, 61.38; H, 6.18. $C_{45}H_{54}FeNi_2Si_4$ (**6** × $C_6H_5CH_3$) requires: C, 61.46; H, 6.54%. MS: $m/z$ 788 ($[M]^+$, 100%), 664 ($[M-CpNi]^+$, 21%), 598 ($[M-Cp_2Ni]^+$, 19%), 544 ($[M-Cp_2NiFe]^+$, 5%), 486 ($[L_2]^+$, 9%), 366 ($[CpNiL]^+$, 35%, 188 ($[Cp_2Ni]^+$, 100%); L is the bridging ligand. The experimental and calculated isotope patterns of $[M]^+$ were in excellent agreement.

### 3.2. Crystal structure determination and MO calculations

Crystals of **6** were obtained as described in the text. The X-ray data were obtained at 205 K from an automated four-circle diffractometer CAD4 (Nonius) working with Mo–$K_\alpha$ radiation ($\lambda = 0.71073$ Å). Crystal data and the data collection parameters are listed in Table 4. The structure was solved and refined by using the program package SHELXTL [17].

The orbitals shown in Fig. 7 were obtained from Extended Hückel calculations by using the program CACAO, version 4.0 [18]. For the input file the crystal data of **6** were averaged in such a way that the molecule had $C_s$ symmetry, and the C–H bond length was assumed to be 1.09 Å.

## 4. Supplementary material

Structural data have been deposited with the Fachinformationszentrum Karlsruhe, CSD No. 406423. Copies of this information may be obtained from FIZ Karlsruhe, D-76344 Eggenstein-Leopoldshafen (e-mail: crystdata@fiz-karlsruhe.de).

## Acknowledgements

Financial support of this work by the Deutsche Forschungsgemeinschft is gratefully acknowledged.

## References

[1] (a) E.W. Neuse, M. Rosenberg, Metallocene Polymers, Marcel Dekker, New York, 1970;
(b) C. Simionescu, T. Lixandru, L. Tataru, I. Mazilu, M. Vata, D. Scutaru, in: J.E. Sheats, C.E. Carraher, Jr., C.U. Pittman (Eds.), Metal-Containing Polymeric Systems, Plenum Press, New York, 1985, p. 89;
(c) P. Ngyen, P. Gómez-Elipe, I. Manners, Chem. Rev. 99 (1999) 1515.
[2] S. Barlow, A.L. Rohl, S. Shi, C.M. Freeman, D. O'Hare, J. Am. Chem. Soc. 118 (1996) 7578.
[3] J. Hiermeier, F.H. Köhler, G. Müller, Organometallics 10 (1991) 1787.
[4] (a) W. Mengele, J. Diebold, C. Röll, H.-H. Brintzinger, Organometallics 12 (1993) 1931;
(b) A. Cano, T. Cuenco, P. Gomez-Sal, B. Royo, P. Royo, Organometallics 13 (1994) 1688;
(c) F.J. Fernándes, P. Gomez-Sal, A. Manzanero, P. Royo, H. Jacobsen, H. Berke, Organometallics 16 (1997) 1553;
(d) T.J. Packham, P. Nguyen, S.C. Bourke, Q. Wang, D.G. Harrison, P. Zoricak, C. Russell, L.M. Liable-Sands, A.L. Rheingold, A.J. Lough, I. Manners, Organometallics 20 (2001) 3035.
[5] (a) F. Amor, P. Gomez-Sal, E. de Jesús, P. Royo, A. Vázques de Miguel, Organometallics 13 (1994) 4322;
(b) J.Y. Corey, J.L. Huhmann, N.P. Rath, Inorg. Chem. 34 (1995) 3203.
[6] (a) M. Fritz, J. Hiermeier, N. Hertkorn, F.H. Köhler, G. Müller, G. Reber, O. Steigelmann, Chem. Ber. 124 (1991) 1531;
(b) H. Atzkern, J. Hiermeier, B. Kanellakopulos, F.H. Köhler, G. Müller, O. Steigelmann, J. Chem. Soc. Chem. Commun. (1991) 997;
(c) U. Siemeling, P. Jutzi, B. Neumann, H.-J. Stammler, Organometallics 11 (1992) 1328;

(d) H. Atzkern, P. Bergerat, H. Beruda, M. Fritz, J. Hiermeier, P. Hudeczek, O. Kahn, F.H. Köhler, M. Paul, B. Weber, J. Am. Chem. Soc. 117 (1995) 997.
[7] B. Grossmann, J. Heinze, E. Herdtweck, F.H. Köhler, H. Nöth, H. Schwenk, M. Spiegler, W. Wachter, B. Weber, Angew. Chem. Int. Ed. Engl. 36 (1997) 387.
[8] A. Haaland, Acc. Chem. Res. 12 (1979) 415.
[9] M. Fritz, J. Hiermeier, F.H. Köhler, Z. Naturforsch. Teil. B 49 (1994) 763.
[10] H. Atzkern, P. Bergerat, M. Fritz, J. Hiermeier, P. Hudeczek, B. Kanellakopulos, O. Kahn, F.H. Köhler, M. Ruhs, Chem. Ber. 127 (1994) 277.
[11] F.H. Köhler, K.H. Doll, W. Prößdorf, Angew. Chem. Int. Ed. Engl. 19 (1980) 479.
[12] G.N. La Mar, J.S. de Ropp, in: L.J. Berliner, J. Reuben (Eds.), NMR of Paramagnetic Molecules (Chapter 1), Plenum Press, New York, 1993, p. 1.
[13] F.H. Köhler, in: J.S. Miller, M. Drillon (Eds.), Magnetism: Molecule to Materials. Models and Experiments (Chapter 12), Wiley-VCH, Weinheim, 2001, p. 379.
[14] H. Atzkern, J. Hiermeier, F.H. Köhler, J. Organomet. Chem. 408 (1991) 281.
[15] P. Baltzer, A. Furrer, J. Hulliger, A. Stebler, Inorg. Chem. 27 (1988) 1543.
[16] R.J. Kurland, B.R. McGarvey, J. Magn. Reson. 2 (1970) 286.
[17] G.M. Sheldrick, Program Package SHELXTL Version 5.1, Universität Göttingen.
[18] C. Mealli, D.M. Proserpio, Chem. Educ. 67 (1990) 399.